PROPAGATION BASED X-RAY PHASE MICROTOMOGRAPHY OF MULTI-MATERIAL OBJECTS FOR SIMULTANEOUS BONE AND SOFT TISSUE VISUALISATION

Max Langer [1,2], Peter Cloetens [2], Bernhard Hesse [2,3], Alexandra Pacureanu [1,2],Kay Raum [3]
Marie-Hélène Lafage-Proust [4], Françoise Peyrin [1,2]

[1]Université de Lyon, CREATIS ; CNRS UMR5220 ; Inserm U1044 ; INSA-Lyon ; Université Lyon 1, F69621 Villeurbanne, France.
[2]European Synchrotron Radiation Facility, F38043 Grenoble Cedex, France
[3]Julius-Wolff-Institute & Berlin Brandenburg School for Regenerative Therapies, Charité-Universitätsmedizin Berlin, D13353 Berlin, Germany
[4]Université de Lyon, LBTO ; Inserm U1059 ; F42034 Saint-Etienne, France

ABSTRACT

We present a method for phase microtomography based on X-ray propagation based phase contrast imaging for multi-material objects. Previously, homogeneous composition assumptions have been in the Radon domain to overcome low sensitivity in the low frequency range. Here, we introduce a prior in the object domain based on multiple, but known, materials in the sample. This is achieved by first reconstructing a tomographic attenuation scan, introducing the prior by segmentation, and finally forward projecting this initial object estimate to yield a priori phase maps. The method is applied to the imaging of a mouse knee where analysis of both soft and hard tissue is of interest, and is shown to perform better than previously proposed methods.

Index Terms— X-ray tomography, phase retrieval, synchrotron radiation, small animal imaging

1. INTRODUCTION

In propagation based X-ray phase tomography, the real part of the refractive index distribution in an object is reconstructed by retrieving the phase of a coherent X-ray beam at several projection angles and using this as input to a tomographic reconstruction algorithm [1]. In the propagation based technique, phase contrast is generated simply by letting the beam propagate in free space after interaction with the object (Fig. 1) [2]. Note the difference to phase contrast tomography, where the raw phase contrast images are used in the tomographic reconstruction.

Several algorithms for phase retrieval from propagation based phase contrast images have been proposed. Most of these are based on linearization of the Fresnel integral to yield efficient algorithms [1, 3-7]. Non-linear, iterative algorithms have also been proposed with the aim to improve spatial resolution of the linear methods, for the radiographic case [8-10], and recently also for tomography [11]. Phase retrieval from propagation based phase contrast images is inherently sensitive to noise in the low frequency range. This is due to weak transfer from low frequencies in the phase shift to the contrast. Low frequency noise compromises quantitative reconstruction of the refractive index and makes interpretation and image analysis, such as segmentation, very difficult without substantial post-treatment. This issue has previously been addressed by introducing a prior on the phase based on a homogeneous composition assumption. This was done by using a scaled version of the attenuation image as an initial guess of the phase. The homogeneity assumption is in the sense of a unique ratio between real and imaginary part of the refractive index, density variations are allowed. This assumes that the composition is known and that an attenuation image can be measured [12].

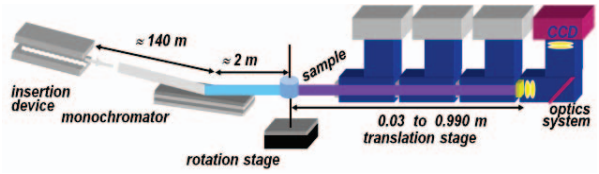


Fig. 1. Experimental setup. Undulator radiation is monochromatized with a multilayer monochromator. The sample is mounted on a translation-rotation stage for tomographic imaging. Imaging is performed with a fluorescent screen CCD based detector, mounted on a translation stage in the beam direction to allow for variation of the free space propagation distance. Phase contrast images are recorded at several sample-to-detector distances. A tomographic scan is recorded at each sample-to-detector distance.

Here, we present an extended regularization approach to allow for multi-material objects, that is heterogeneous objects consisting of several defined materials. Such a prior can not be introduced directly in the projections, as there are several unknowns in the phase map as well as the attenuation map: the distance traveled in each material, and the real and complex part of the refractive index respectively. Instead, it has to be introduced in the object domain. We propose to do this by first reconstructing the attenuation index from acquired projection images, thresholding this reconstruction to calculate a 3D δ/β-map, applying this map on the reconstructed attenuation index to yield an a priori refractive index guess, and finally forward projecting this prior refractive index, which yields a prior estimate on the phase shift at each projection angle.

The method is applied to the imaging of a mouse knee. Small animal models of osteoarthritis are often used for evaluating treatments and cartilage repair strategies. Non-invasive techniques are limited by the joint size and the low radio opacity of soft

tissues. We demonstrate the proposed methods ability to resolve both hard and soft tissues.

2. FORWARD PROBLEM

If we consider a monochromatic, coherent, parallel X-ray beam, the interaction of the beam with the object can be described by its complex refractive index

$$n(\mathbf{r}) = 1 - \delta_n(\mathbf{r}) - i\beta(\mathbf{r}), \quad (1)$$

where $\mathbf{r} = (r, s, t)$ are the spatial coordinates in the object domain. Both phase shift and absorption of the beam by the object at a certain projection angle θ can be described by straight line projections through the refractive index so that

$$B_\theta(\mathbf{x}) = (2\pi/\lambda) \int_{(\theta,\mathbf{x})\ \text{line}} \beta_n(\mathbf{r}) \mathrm{d}z \quad (2)$$

and

$$\varphi_\theta(\mathbf{x}) = -(2\pi/\lambda) \int_{(\theta,\mathbf{x})\ \text{line}} \delta_n(\mathbf{r}) \mathrm{d}z \quad (3)$$

where $z = r\cos\theta + s\sin\theta$ is the propagation direction of the X-rays. The beam interaction with the object can then be described by a transmittance function

$$T_\theta(\mathbf{x}) = a_\theta(\mathbf{x}) \exp[i\varphi_\theta(\mathbf{x})] = \exp[-B_\theta(\mathbf{x}) + i\varphi_\theta(\mathbf{x})] \quad (4)$$

Letting the beam propagate in free space over a distance D after interaction with the object can be described by the Fresnel transform [14]

$$T_{\theta,D}(\mathbf{x}) = Fr_D[T(\mathbf{x})] \quad (5)$$

What is registered on the detector, however, is the intensity $I_D(\mathbf{x})$ of the wavefield. If we assume a uniform incident beam, we have

$$I_D(\mathbf{x}) = \left|T_{\theta,D}(\mathbf{x})\right|^2 + \gamma(\mathbf{x}) \quad (6)$$

where $\gamma(\mathbf{x})$ describes noise and other imperfections in the image, however these contributions are not necessarily additive or uncorrelated with the object. Putting the detector in the object contact plane so that $D = 0$ yields directly the attenuation image

$$I_0(\mathbf{x}) = a_\theta^2(\mathbf{x}) + \gamma(\mathbf{x}). \quad (7)$$

3. INVERSE PROBLEM

Reconstruction of the 3D refractive index is considered as a two-step process. The phase shift is first retrieved at each projection angle, a 2D problem. The retrieved phase maps are then used as input to a tomographic reconstruction algorithm. The phase shift can be reconstructed from a series
of images at different distances by solving the minimization problem

$$\hat{\varphi}_\theta(\boldsymbol{x}) = \arg\min \sum_D \left|\tilde{I}_{\theta,D,\varphi}(\mathbf{x}) - I_{\theta,D}(\mathbf{x})\right|^2 + \alpha\left|\varphi_\theta(\mathbf{x}) - \varphi_{\theta,0}(\mathbf{x})\right|^2 \quad (8)$$

where $\tilde{I}_{\theta,D,\varphi}(\mathbf{x})$ is the intensity calculated with some model such as the mixed approach [5] and $\varphi_0(\mathbf{x})$ is an a priori known solution.

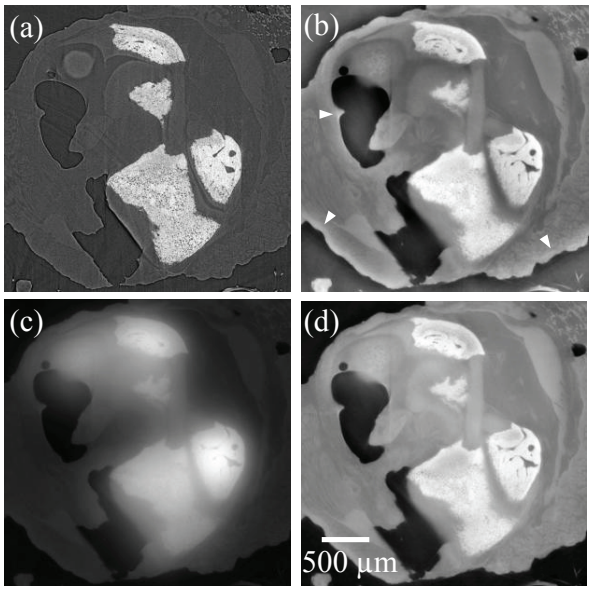


Fig. 2. Reconstructions of transverse slices in the mouse knee joint. (a) Standard attenuation-based reconstruction. Contrast is good in the hard tissue but weak in the soft tissue. (b) Phase tomography reconstruction using the homogeneous composition prior with the δ/β-ratio set to correspond to bone. Contrast is greatly improved, details in the soft tissue such as ligaments, cartilage and muscle are visible. However, artifacts are present on the border of the soft tissue (indicated with arrowheads). (c) Phase tomography reconstruction using the homogeneous composition prior, δ/β-ratio set to correspond to soft tissue. The artifact on the edge of soft tissue is alleviated, but instead there are swelling artifacts in the bone (d) Phase reconstruction with the proposed method. Both types of artifacts are alleviated.

4. DESIGN OF THE A PRIORI

Previously, $\varphi_0(\mathbf{x})$ has been set to 0, which stabilizes the problem but is sensitive to low frequency noise [5]. Setting $\varphi_{\theta,0}(\mathbf{x})$ proportional to $B_{\theta,0}(\mathbf{x})$ has also been reported [11]. This yields

$$\varphi_{\theta,0}(\mathbf{x}) = \mathrm{f}(\mathbf{x}) * \frac{\delta_n}{2\beta} \ln\left[\mathrm{I}_{\theta,0}(\mathbf{x})\right], \quad (9)$$

where $f(\mathbf{x})$ is a low-pass filter so that the prior is introduced in the low frequency range only. While this has proved to be useful in practice (e.g., [15]), the homogeneity assumption can be restrictive (Fig 2b, c). Instead, the δ/β-ratio should vary across the projection. This is not possible to introduce directly in the projection images however, since the path length in each material is still unknown.

To avoid this problem, we propose to introduce the a priori knowledge in the object domain. This allows choosing the δ/β-ratio as a function of β, hence letting it vary across the sample. This way of introducing the prior allows considerable flexibility in its design. Constructing such a prior requires the measurement of an attenuation scan, however in the case of the mixed approach, this has to be recorded anyway [5]. Reconstructing $\beta(\mathbf{r})$ from $I_{\theta,0}(\mathbf{x})$ yields

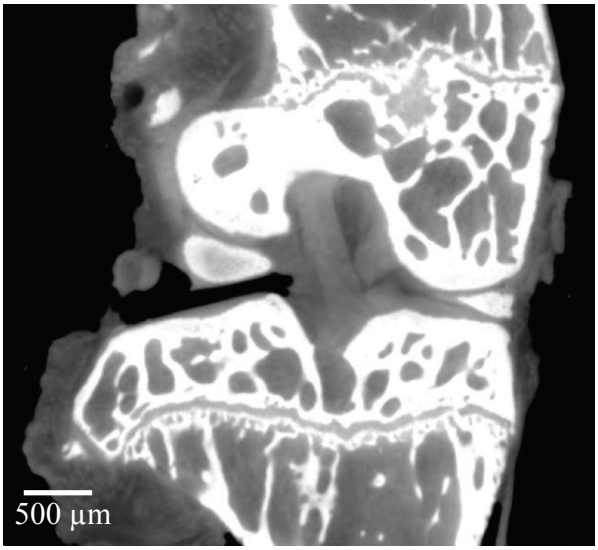


Fig. 3. Sagittal slice through the mouse knee reconstructed with the proposed method, windowed to show the soft tissue. Mineralized and soft parts of the meniscus, as well as articular cartilage and cruciate ligaments can be seen.

$$\hat{\beta}(\mathbf{r}) = \beta(\mathbf{r}) + \Gamma(\mathbf{r}), \tag{10}$$

where $\Gamma(\mathbf{r})$ is due to noise and other imperfections in $\gamma(\mathbf{x})$. $\hat{\beta}(\mathbf{r})$ is thresholded to separate the object into hard and soft tissue. Different linear or non-linear image enhancement techniques can be envisaged, such as denoising and ring removal, to facilitate the thresholding thereby acquiring a better a priori estimate. We let any such operations be represented by the function $g[\beta(\mathbf{r})]$ acting on the object so that

$$m(\mathbf{r}) = \begin{cases} \delta_a/\beta_a & g[\hat{\beta}(\mathbf{r})] > t \\ \delta_b/\beta_b & \text{otherwise} \end{cases}. \tag{11}$$

$\beta_a > \beta_b$ and δ_a, δ_b are *a priori* known components of the refractive index, which assumes that the approximate composition of the sample is known, and $\beta_a > t > \beta_b$ is the chosen threshold. The prior estimate of $\delta(\mathbf{r})$ is obtained as

$$\delta_0(\mathbf{r}) = m(\mathbf{r})\hat{\beta}(\mathbf{r}). \tag{12}$$

To construct the *a priori* phase maps, the object prior estimate is forward projected as

$$\varphi_{\theta,0}(\mathbf{x}) = -(2\pi/\lambda) \int_{(\theta,\mathbf{x})\ \text{line}} \delta_0(\mathbf{r}) \mathrm{d}z. \tag{13}$$

These *a priori* phase maps are introduced in the low frequency range only as before (Eq. 9) by the application of a low pass filter $f(\mathbf{x})$.

5. EXPERIMENT

A mouse rear left limb was excised, stripped of skin and external musculature and fixed in formaldehyde. The sample was removed from the formaldehyde and mounted in a PMMA tube for imaging. Projection data was acquired at the ID19 beamline at the European Synchrotron Radiation Facility (ESRF), Grenoble, France. X-ray energy was set to 30 keV, selected from wiggler radiation with a double Si-crystal monochromator set to reflect in the vertical plane. Images were recorded at 2000 angles of view over a 180° rotation of the sample. Such scans were recorded at 3 sample-to-detector distances (D=[60 300 1000] mm). A 2048×2048 pixels CCD detector with a 200 µm LuAg fluorescent screen was used, with effective pixel size set to 5 µm. Tomographic reconstruction based on FBP and forward projection was performed using in-house software (PyHST) [15].

Phase retrieval was performed using $\delta_a/\beta_a = 543$ (bone, cortical (ICRU-44)), $\delta_b/\beta_b = 2035$ (tissue, soft (ICRU-44)). These values were calculated using the XOP software [17]. $g(\mathbf{r})$ was implemented as an 11×11 2D median filter in the transverse slices, and the threshold $4\pi t/\lambda$ was set to 1.1 cm^{-1}, selected with Otsu's method. The regularizing parameter α was set automatically using the L-curve criterion [12].

6. RESULTS

Reconstructed transverse slices through the knee joint are shown in Fig. 2. The attenuation reconstruction (Fig. 2a) yields correctly reconstructed hard tissues, but contrast in soft tissue is low. Reconstruction using the homogeneous object approach [12] show artifacts that could be problematic for further analysis. If the δ/β-ratio is set to correspond to bone, the hard tissue is correctly reconstructed, but ringing artifacts are present in the soft tissue, especially on the tissue-air interface (Fig. 2b). This is due to the δ/β-ratio being set too low in the soft tissue. If the δ/β-ratio instead is set to correspond to soft tissue, the ringing artifacts on the tissue-air interface are alleviated and soft tissue contrast is improved, but here there are strong swelling artifacts in the hard tissue parts, due to the chosen δ/β-ratio being too high there (Fig. 2c). In the reconstruction with the proposed method, both these artifacts are alleviated (Fig. 2d). Gray level is proportional to local mass density.

A sagittal slice is shown in Fig. 3, windowed to show soft tissue. Soft tissue detail is clearly visible, such as cruciate ligaments, meniscus and articular cartilage. A volume rendering of the joint is shown in Fig. 4. The reconstructed volume should permit morphological measurement of bone and soft tissue compartments, such as thickness of articular cartilage and mineralization of the bone.

7. DISCUSSION AND CONCLUSION

In this paper we proposed a phase retrieval algorithm in the X-ray propagation based phase contrast framework where a priori information is introduced in the object domain. This extends previous algorithms assuming homogeneous objects, and alleviates associated artifacts. The algorithm was applied to the imaging of a mouse knee where it permits quantitative imaging of the electron density in both soft and hard tissue. Quantitative evaluation of the algorithm has been presented elsewhere [18].

There is accumulating evidence from the literature that pathophysiology of osteoarthritis involves subchondral bone, even at earlier stages of the disease. However, so far, no imaging technique has been able to assess, at high resolution, both morphology of articular cartilage and its underlying bone in rodent models especially in mice. Contrast agent enhanced micro-computed tomography has been used to study structural as well as functional aspects of the articular cartilage [19]. Magnetic

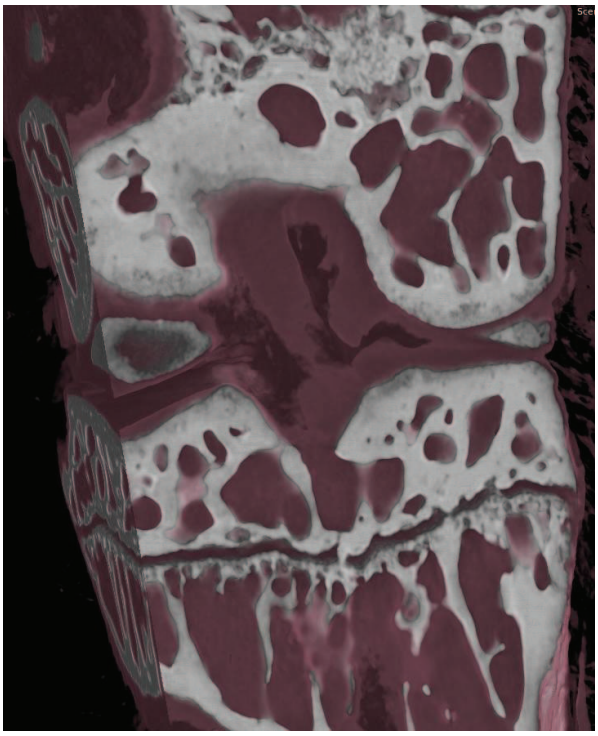


Fig. 4. Volume rendering of a virtual cut in the mouse knee. Bone as well as soft tissue is well reconstructed. Soft tissue detail is clearly visible, such as cruciate ligaments, mineralized and cartilaginous meniscus and articular cartilage.

resonance imaging at the micrometric scale has also been performed but lacks spatial resolution for imaging of small animal models [20]. The proposed method allows quantitative imaging in terms of tissue density of both bone and cartilage simultaneously and without contrast agent, while providing spatial resolution down to the sub-micrometer level. The first results presented here shows great promise of the method to be used for the study of bone and cartilage density and morphology which would be very valuable in the study of degenerative disease such as osteoarthritis.

Some resolution is lost in the phase retrieval process, but the resulting tomograms show very high signal to noise ratio. Since the algorithm is sensitive to the choice of δ/β-ratios, the composition of the sample has to be known. Future work includes improving spatial resolution by application of non-linear phase retrieval algorithms.

8. REFERENCES

[1] P. Cloetens, W. Ludwig, J. Baruchel, D. Van Dyck, J. Van Landuyt, J. P. Guigay, and M. Schlenker, "Holotomography: Quantitative phase tomography with micrometer resolution using hard synchrotron radiation X rays," *Appl. Phys. Lett.*, vol. 75, pp. 2912-2914, 1999.

[2] A. Snigirev, I. Snigireva, V. Kohn, S. Kuznetsov, and I. Schelokov, "On the possibilities of X-ray phase contrast microimaging by coherent high-energy synchrotron radiation," *Rev. Sci. Instrum.,* vol. 66, pp. 5486-5492, 1995.

[3] K. A. Nugent, T. E. Gureyev, D. F. Cookson, D. Paganin, and Z. Barnea, "Quantitative phase imaging using hard X rays," *Phys. Rev. Lett.,* vol. 77, pp. 2961-2964, 1996.

[4] D. Paganin, S. C. Mayo, T. E. Gureyev, P. R. Miller, and S. W. Wilkins, "Simultaneous phase and amplitude extraction from a single defocused image of a homogeneous object," *J. Microsc.,* vol. 206, pp. 33-40, 2002.

[5] J. P. Guigay, M. Langer, R. Boistel, and P. Cloetens, "A mixed contrast transfer and transport of intensity approach for phase retrieval in the Fresnel region," *Opt. Lett.,* vol. 32, pp. 1617-1619 (2007).

[6] M. Langer, P. Cloetens, J. P. Guigay, and F. Peyrin, "Quantitative comparison of direct phase retrieval algorithms in in-line phase tomography," *Med. Phys.*, vol. 35, pp. 4556-4566, 2008.

[7] X. Wu. H. Liu, A. Yan, "X-ray phase-attenuation duality and phase retrieval," *Opt. Lett.,* vol. 30, pp. 379-291, 2005.

[8] L. J. Allen and M. P. Oxley, "Phase retrieval from from series of images obtained by defocus variation," *Opt. Comm.,* vol. 199, pp. 65-75, 2001.

[9] V. Davidoiu, B. Sixou, M. Langer, and F. Peyrin, "Non-linear iterative phase retrieval based on Frechet derivative," *Opt. Express,* vol. 19, pp. 22809-22819, 2011.

[10] J. Moosmann, R. Hofmann, A. Bronnikov, and T. Baumbach, Opt. Express **18**, 25771 (2010).

[11] M. Langer, A. Pacureanu, P. Cloetens, Q. Grimal, and F. Peyrin, "X-ray phase nanotomography resolves the 3D human bone ultrastructure," *PLoS One*, submitted.

[12] M. Langer, P. Cloetens, and F. Peyrin, "Regularization of phase retrieval with phase-attenuation duality prior for 3D holotomography," *IEEE Trans. Image Process.,* Vol. 19, pp. 2428-2436, 2010.

[13] M. A. Beltran, D. M. Paganin, K. Uesugi, and M. J. Kitchen, "2D and 3D X-ray phase retrieval of multi-material objects using a single defocus distance," *Opt. Express,* vol. 18, pp. 6423-6436, 2010.

[14] J. W. Goodman, *Introduction to Fourier optics* (Roberts, 2005).

[15] M. Langer, Y. Liu, F. Tortelli, P. Cloetens, R. Cancedda, and F. Peyrin, "Regularized phase tomography enables study of mineralized and unmineralized tissue in porous bone scaffold," *J. Microsc.,* vol. 238, pp. 230-239, 2010.

[16] J. Banhart, *Advanced tomographic methods in materials research and engineering* (Oxford University Press, 2008).

[17] R. J .Dejus and M. Sanchez del Rio, "XOP: A graphical user interface for spectral calculations and X-ray optics utilities," *Rev. Sci. Instrum.*, vol. 67, pp. 3356, 1996.

[18] M. Langer, P. Cloetens, A. Pacureanu, and F. Peyrin, "X-ray in-line phase tomography for multi-material objects," *Opt. Lett.*, submitted.

[19] A. W. Palmer, R. E. Guldberg, and M. E. Levenston, "Analysis of cartilage matrix fixed charge density and three-dimensional morphology via contrast-enhanced microcomputed tomography," *Proc. Natl. Acad. Sci. U. S. A.*, vol. 103, pp. 19255-19260, 2006.

[20] R. Bolbos, H. Benoit-Cattin, J. B. Langlois, A. Chomel, E. Chereul, C. Odet, P. Pastoreau, M. Janier, and O. Beuf, "Knee cartilage thickness measurements using MRI: a 4 1/2-month longitudinal study in the meniscectomized guinea pig model of OA," *Osteoarthr. Cartilage,* vol. 15, pp. 656-665, 2007.